THE JOURNAL OF BIOLOGICAL CHEMISTRY VOL. 289, NO. 41, pp. 28505–28512, October 10, 2014
Published in the U.S.A.

The Roles of the RIIβ Linker and N-terminal Cyclic Nucleotide-binding Domain in Determining the Unique Structures of the Type IIβ Protein Kinase A

A SMALL ANGLE X-RAY AND NEUTRON SCATTERING STUDY[*] [◆]

Received for publication, May 23, 2014, and in revised form, August 4, 2014 Published, JBC Papers in Press, August 11, 2014, DOI 10.1074/jbc.M114.584177

Donald K. Blumenthal[‡1,2], **Jeffrey Copps**[§1,3], **Eric V. Smith-Nguyen**[§], **Ping Zhang**[§], **William T. Heller**[¶], **and Susan S. Taylor**[§‖]

From the [‡]*Department of Pharmacology and Toxicology, University of Utah, Salt Lake City, Utah 84112, the* [§]*Howard Hughes Medical Institute and Department of Chemistry and Biochemistry, University of California, San Diego, La Jolla, California 92093-0654, the* [¶]*Biology and Soft Matter Division, Oak Ridge National Laboratory, Oak Ridge, Tennessee 37831, and the* [‖]*Department of Pharmacology, University of California, San Diego, La Jolla, California 92093-0654*

Background: The RIIβ subunit of PKA exhibits unique isoform-specific structural features.
Results: The unique structural properties of RIIβ do not require the C-terminal cAMP-binding domain.
Conclusion: The RIIβ linker and N-terminal cAMP-binding domain confer unique subunit structure and organization of the type IIβ holoenzyme.
Significance: The subunit structure and organization of the type IIβ holoenzyme contribute to its unique isoform-specific biochemical properties and functions.

Protein kinase A (PKA) is ubiquitously expressed and is responsible for regulating many important cellular functions in response to changes in intracellular cAMP concentrations. The PKA holoenzyme is a tetramer (R_2:C_2), with a regulatory subunit homodimer (R_2) that binds and inhibits two catalytic (C) subunits; binding of cAMP to the regulatory subunit homodimer causes activation of the catalytic subunits. Four different R subunit isoforms exist in mammalian cells, and these confer different structural features, subcellular localization, and biochemical properties upon the PKA holoenzymes they form. The holoenzyme containing RIIβ is structurally unique in that the type IIβ holoenzyme is much more compact than the free RIIβ homodimer. We have used small angle x-ray scattering and small angle neutron scattering to study the solution structure and subunit organization of a holoenzyme containing an RIIβ C-terminal deletion mutant (RIIβ(1–280)), which is missing the C-terminal cAMP-binding domain to better understand the structural organization of the type IIβ holoenzyme and the RIIβ domains that contribute to stabilizing the holoenzyme conformation. Our results demonstrate that compaction of the type IIβ holoenzyme does not require the C-terminal cAMP-binding domain but rather involves large structural rearrangements within the linker and N-terminal cyclic nucleotide-binding domain of the RIIβ homodimer. The structural rearrangements are significantly greater than seen previously with RIIα and are likely to be important in mediating short range and long range interdomain and intersubunit interactions that uniquely regulate the activity of the type IIβ isoform of PKA.

The ubiquitously expressed cAMP-dependent protein kinase, otherwise known as protein kinase A (PKA), regulates many vital cellular functions including glycogen metabolism (1), calcium flux in cardiac muscle cells (2), synaptic transmission and plasticity in neurons (3), and the expression of many proteins via the activation of the cAMP-response element-binding protein (CREB) (4). Like all protein kinases, PKA acts as a molecular switch at critical biochemical junctions, phosphorylating ion channels and receptors at the plasma/mitochondrial membranes, as well as other substrates in response to increasing cellular cAMP levels, thus altering their functions. Not surprisingly, aberrant PKA activity is implicated in a variety of diseases including Carney complex (5), Cushing syndrome (6–10), breast and liver cancer (11–14), myocardial hypertrophy, atrial fibrillation, and long QT syndrome (15–17), as well as several neurodegenerative disorders (18–20).

PKA forms an inactive tetrameric holoenzyme, consisting of a regulatory subunit homodimer (R2) and two catalytic (C) subunits. The R subunits bind to the C subunits and inhibit their catalytic activity. cAMP binding to the R subunits activates the C subunits by removing inhibitory interactions. Because PKA functions as a complex of regulatory and catalytic subunits and not a single chain enzyme, it can assume many and varied cellular functions throughout the body. In mammalian cells, there are four isoforms of the R subunit: two broad classes of R subunit, RI and RII, each consisting of α and β isoforms (RIα, RIβ, RIIα, RIIβ). All of the R subunit isoforms are similar in overall

* This work was supported in part by National Institutes of Health Grant GM34921 (to S. S. T.). A portion of this research was sponsored in part by the Laboratory Directed Research and Development Program at Oak Ridge National Laboratory, managed by UT-Battelle, LLC, for the U. S. Department of Energy (to W. T. H.).
◆ This article was selected as a Paper of the Week.
[1] Both authors contributed equally to this work.
[2] To whom correspondence should be addressed: Dept. Pharmacology and Toxicology, University of Utah, 30 S. 2000 E., Rm. 201, Salt Lake City, UT 84112. Tel.: 801-585-3094; Fax: 801-585-5111; E-mail: don.blumenthal@pharm.utah.edu.
[3] Present address: Dept. of Integrative Structural and Computational Biology, The Scripps Research Institute, 10550 N. Torrey Pines Rd., La Jolla, CA 92037.

domain structure. Each R subunit contains a dimerization/docking (D/D)[4] domain at the N terminus followed by a conformationally flexible linker sequence and then a pair of highly conserved cyclic nucleotide-binding domains (CNBD-A and CNBD-B) at the C terminus. Recent studies have shown that the R subunit linker region is a dynamic structural element that plays a critical allosteric role in regulating PKA activation and is not simply a passive covalent element connecting the D/D and CNBD-A domains (21). A short sequence within the linker known as the inhibitory site motif binds in the substrate-binding site of the C subunit and inhibits C subunit activity. In the RII isoforms, the inhibitory site motif contains a serine that can be autophosphorylated by the C subunit in the holoenzyme complex. As shown by several different crystal structures of PKA R:C heterodimers and R_2:C_2 holoenzymes solved in our laboratory, the arrangement of the CNBD domains and the structural changes that they undergo upon cAMP binding contribute to their isoform-specific differences in C subunit activation (22). The structural differences in the D/D domain among these R subunit isoforms confer additional and unique subcellular targeting and other functional differences to each type of PKA holoenzyme (23). For example, type I PKA holoenzymes (those containing RI homodimers) are typically diffusely distributed in the cytosol, whereas type II holoenzymes are largely targeted to signaling complexes at membranes and other subcellular sites. The localization of PKA holoenzymes is conferred by the R subunit homodimer D/D domains, which bind with high affinity to A-kinase anchoring proteins (AKAPs). AKAPs contain localization motifs, binding sites for PKA, and can also act as scaffolds for other signaling proteins such as protein phosphatases, cyclic nucleotide phosphodiesterases, and adenylate cyclases (24). AKAP-mediated signaling complexes can thus serve to integrate and coordinate the regulation of ion channels, cytoskeletal and contractile proteins, metabolic enzymes, and other proteins in response to changes in cAMP, Ca^{2+}, and other intracellular signals.

Small angle x-ray scattering (SAXS) experiments support the notion that each of the R isoforms confers unique structural attributes to the solution structure of the four different PKA isoforms. These studies have also provided a window into the conformational changes that take place in the R subunit homodimer upon holoenzyme association and dissociation. SAXS has shown that the solution structures of free RI homodimers are compact structures, whereas the RII homodimers are extended. The type Iα tetrameric holoenzyme remains relatively compact upon binding C subunits (25), whereas the type Iβ tetrameric holoenzyme is considerably more extended (26). In contrast, the type IIα holoenzyme is very extended, whereas the type IIβ holoenzyme is unique among the isoforms in that it is much more compact than the free RIIβ homodimer (22, 27). These differences in structural behavior among the R subunit isoforms are in large part attributable to differences in their respective linker regions, the regions of greatest sequence variability and length among the isoforms.

To better understand how the several RIIβ homodimer domains contribute to the solution structure of the type IIβ holoenzyme, we have used SAXS and small angle neutron scattering (SANS) to characterize global structure and subunit organization of a holoenzyme formed using an RIIβ truncation mutant, RIIβ(1–280), that is missing the CNBD-B domain. The complex formed with the RIIβ(1–280) homodimer has the minimal domain structure needed to form an R_2:C_2 type IIβ holoenzyme complex. Moreover, the RIIβ(1–280) homodimer has an affinity for the C subunit (K_D = 26 nM) that is only 4-fold lower than full-length RIIβ homodimer (28). SANS with solvent contrast variation is a solution structural method that has been used to reveal the subunit organization of the type IIα and type Iα holoenzymes (25, 29), as well as other multiprotein assemblies, by using complexes formed with specifically deuterated proteins (30). Because of the large difference in the scattering length density of neutrons for hydrogen and deuterium atoms, the hydrogenated and perdeuterated subunits give different scattering intensities relative to solvent as the D_2O content is varied. Using SANS with solvent contrast variation, the individual scattering intensities of the hydrogenated and perdeuterated subunits in a multisubunit protein complex can be resolved, revealing the conformation and position of subunits within the complex. We describe here the use of the RIIβ(1–280) construct to reveal important insights into the unique structural rearrangements that occur during the activation and inactivation of the type IIβ holoenzyme as compared with other PKA isoforms.

EXPERIMENTAL PROCEDURES

Protein Mutagenesis, Expression, and Purification—Recombinant rat RIIβ(1–280) was prepared from a full-length rat RIIβ construct in the pRSET B expression cassette as described previously (28). RIIβ(1–280) protein was expressed and purified in a manner identical to wild-type and mutant full-length RIIβ (31). For SAXS experiments, recombinant wild-type hydrogenated mouse C subunit was expressed and purified as described previously (32). To express deuterated wild-type mouse C subunit for SANS experiments, 10 liters of LB medium were inoculated with BL21 DE3 transfected with the C subunit expression vector. The 1-liter flasks were aerated in a 37 °C incubator until the A_{600} reached 1.0. The cells were spun down gently in a centrifuge at 2400 rpm. Each pellet was resuspended in 500 ml of M9 medium containing 80% D_2O and 20% H_2O. The pellets were placed in an incubator at room temperature and allowed to recover for 1 h. The cells were then induced with isopropyl β-D-1-thiogalactopyranoside and incubated overnight at 16 °C. Cells were harvested and lysed, and C subunit was purified as described previously (32). Type IIβ(1–280) holoenzymes were formed in the same manner as described previously for type IIβ full-length holoenzymes (31).

SAXS—SAXS data were acquired at the University of Utah using a SAXSess (Anton Paar) line collimation (10-mm) instrument. Samples were maintained at 12 °C in 1-mm internal diameter quartz capillary cells. Data were collected using an image plate detector and reduced to $I(q)$ *versus* q

[4] The abbreviations used are: D/D, dimerization/docking; CNBD, cyclic nucleotide-binding domain; AKAP, A-kinase anchoring protein; D_{max}, maximum particle dimension; $I(q)$, scattering intensity at angle q; R_g, radius of gyration; SANS, small angle neutron scattering; SAXS, small-angle X-ray scattering.

$$q = (4\pi\sin\theta)/\lambda \quad \text{(Eq. 1)}$$

where 2θ is the scattering angle and $\lambda = 1.54$ Å CuKα) using the program SAXSquant 2.0 (Anton Paar). X-ray scattering from the protein was obtained by subtracting the scattering of the normalized buffer blank. The distance distribution function, $P(r)$, was calculated as the inverse Fourier transform of $I(q)$ *versus* q data using the program GNOM (33), which employs an indirect transform approach. Data were corrected for slit-smearing effects in GNOM using beam length profile parameters determined at the time of data collection. In addition to $P(r)$, GNOM also provides an estimate of the radius of gyration, R_g. The value of D_{max}, the maximum linear dimension of the particle, was estimated using goodness of fit parameters provided by GNOM and by visual assessment of the $P(r)$ curves determined using multiple trial estimates of D_{max}.

SANS with Solvent Contrast Variation—SANS data were collected at the Oak Ridge National Laboratory (ORNL) using the CG3 (Bio-SANS) instrument (34) at the High Flux Isotope Reactor (HFIR). For the SANS measurements, samples were loaded into 0.1-cm path length quartz cuvettes (Hellma USA, Inc.) and maintained at 18 °C in the sample changer of the instrument by means of a water bath. Solvent contrast series experiments were performed using nominal D_2O concentrations of 0, 10, 20, and 100%. Accurate D_2O/H_2O ratios were determined after data collection using neutron transmission data as described previously (25). To collect data over a sufficient q-range for the data reduction and analysis, data were collected from two configurations of the instrument, sample-to-detector distances of 1.1 and 6.8 m. The measurements utilized a wavelength of 6.0 Å, and the wavelength spread, $\Delta\lambda/\lambda$, was set to 0.15.

Data reduction followed standard procedures to correct for detector sensitivity, dark current (cosmic radiation background and detector electronic noise), geometric effects, sample transmission, and solvent background. Reduced data were than azimuthally averaged to produce the one-dimensional scattering intensity profile. The data from the two instrument configurations were merged using routines developed by the National Institute of Standards and Technology in the IgorPro software package (WaveMetrics, Inc.) (35).

Subsequent analysis of individual scattering curves for R_g was done using PRIMUS (36). The MULCh web server (37) was used to analyze the R_g of the components from the contrast variation series data and to extract the basic scattering functions of each of the deuterated and hydrogenated components from the contrast series. GNOM (33) was used for the $P(r)$ curves from the basic scattering functions.

Structural models of the isotopically labeled subunits were determined from the SANS data using a rigid body modeling approach built around the program ORNL_SAS (38). The rigid body modeling of the RIIβ(1–280) holoenzyme followed the approach employed previously by Heller *et al.* (25) using the D/D domain of RIIα (Protein Data Bank (PDB): 2HWN), a single cylindrical volume to simulate the volume occupied by the flexible linkers, and the R:C heterodimer structure taken from the crystal structure of the RIIβ holoenzyme (PDB: 3TNP) in which the structures of the CNBD-B domains were deleted from the PDB file. The two R:C heterodimers were allowed to have arbitrary rotation about the N terminus of the R subunit, which was constrained to contact the linker cylinder. A two-fold axis of symmetry about the axis of symmetry of the D/D domain was imposed on the entire model. The cylinder height and rotation angles of the models were chosen through a Monte Carlo process. Models were checked for structural overlap of the various substructures, and those having too many unfavorable collisions were not tested against the SANS data using ORNL_SAS. A continuously updated set of the 25 best models found was output by the program to provide a measure of the variability of the range of models found that fit the data, as employed previously (39). Three independent runs of the modeling were performed, providing a set of 75 models for judging the variability and convergence of the modeling results.

RESULTS

Characterization of Type IIβ(1–280) Holoenzyme by SAXS—Prior to analysis of the type IIβ(1–280) holoenzyme by SANS, the scattering of holoenzyme complexes reconstituted with deuterated C and hydrogenated C were characterized by SAXS. The $I(q)$ *versus* q scattering curves, Guinier plots, and corresponding $P(r)$ curves are shown Fig. 1. The scattering curves of the type IIβ(1–280) holoenzyme complexes formed with deuterated C and hydrogenated C were nearly identical, indicating that deuteration had minimal effects on the solution structure of the holoenzyme complex. The basic scattering parameters (Table 1) indicate that the type IIβ(1–280) holoenzyme is compact (R_g = 37.8 Å, D_{max} = 115 Å) and is smaller than the holoenzyme complex containing full-length RIIβ (R_g = 46.2Å and D_{max} = 145 Å). The shorter maximal distance of the type IIβ(1–280) holoenzyme is thus partly due to the lack of the C-terminal CNBD-B domains in RIIβ(1–280).

SANS Analysis of Type IIβ(1–280) Holoenzyme—SANS with contrast variation was used to determine the domain and subunit organization of type IIβ(1–280) holoenzyme reconstituted with hydrogenated RIIβ(1–280) homodimer and deuterated C subunit. The SANS data were collected at four different solvent contrast points, 0, 10, 20, and 100% D_2O (Fig. 2*A*). The solvent contrast series was analyzed using MULCh to extract information regarding the scattering intensity profiles of the individual components of the holoenzyme complex (the RIIβ(1–280) homodimer and the two C subunits) and the relative positions of the subunits in the complex.

The R_g analysis component of MULCh performs a Stuhrmann analysis (40) and a parallel axis analysis that provides information about the R_g of each component (R1 and R2) of the complex and the R_g of the complex at infinite contrast. The R_g values of the RIIβ(1–280) homodimer (R1) in the type IIβ(1–280) holoenzyme were estimated to be 36.77 ± 1.23 and 36.76 ± 1.20 Å by Stuhrmann and parallel axis analysis, respectively, and the R_g values of the two C subunits were 37.10 ± 1.95 and 37.10 ± 1.97 Å, respectively. The Stuhrmann value of R_m, the R_g of the complex at infinite contrast (37.42 ± 1.07 Å), is in good agreement with the R_g of the complex estimated from SAXS (36.7 ± 0.15 Å for the complex with deuterated C subunit and 37.8 ± 0.22 Å for hydrogenated C, Table 1).

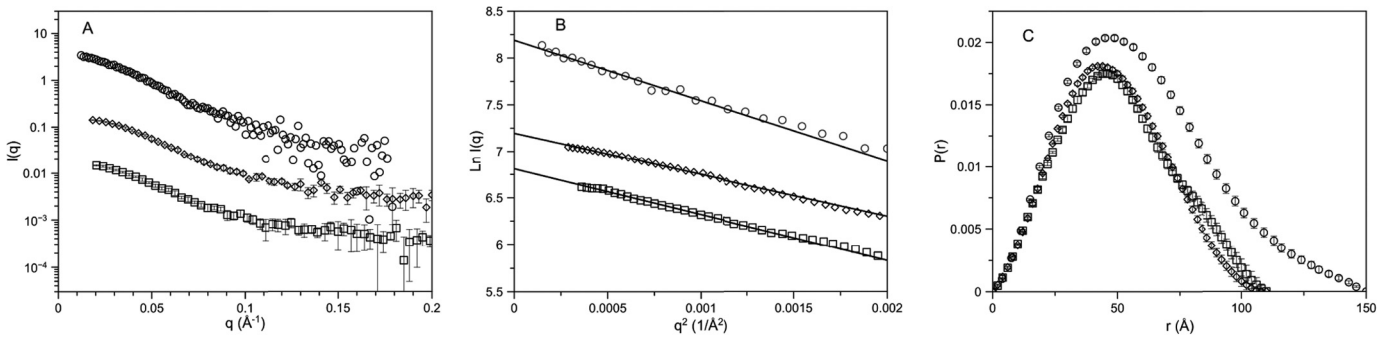

FIGURE 1. **Small angle x-ray scattering of RIIβ(1–280) holoenzyme as compared with full-length RIIβ holoenzyme.** *A*, *I*(*q*) *versus q* plots of RIIβ(1–280) holoenzyme formed with hydrogenated C subunit (*open squares*) and with deuterated C subunit (*open diamonds*). The scattering data were binned, and the *error bars* reflect the S.D. of the data within the bin. The *I*(*q*) *versus q* plot of full-length RIIβ holoenzyme (from Vigil *et al.* (31)) is shown for comparison (*open circles*). The *I*(*q*) scale is arbitrary, and the plots have been offset to facilitate comparison. *B*, Guinier plots of RIIβ(1–280) holoenzyme formed with hydrogenated C subunit (*open squares*) and deuterated C subunit (*open diamonds*) as compared with full-length RIIβ holoenzyme (*open circles*). The *I*(*q*) scale is arbitrary and has been offset to facilitate comparison. The line shown with each dataset is a linear fit to the data in the range from q_{min} to $q^2 = 0.0013$. This value of q^2 corresponds to $q \times R_g = 1.3$. *C*, pairwise length distance distribution curves of RIIβ(1–280) holoenzyme formed with hydrogenated C subunit (*open squares*) and deuterated C subunit (*open diamonds*) as compared with full-length RIIβ holoenzyme (*open circles*). The area under each curve has been scaled to reflect the square of molecular weight of the particle. Estimated errors are equal to or smaller than the symbols.

TABLE 1

Basic scattering parameters of type IIβ holoenzymes and RIIβ homodimers

Protein	D_{max}	R_g [a]
	Å	*Å*
Type IIβ(1–280) deuterated C holoenzyme	110	36.7 ± 0.15
Type IIβ(1–280) hydrogenated C holoenzyme	115	37.8 ± 0.22
Type IIβ (full-length) holoenzyme[b]	145	46.2 ± 0.5
Free RIIβ(1–280) homodimer (SAXS)	140	43.4 ± 0.44
Holoenzyme-bound RIIβ(1–280) homodimer (SANS)	110	35.6 ± 0.15
Free RIIβ (full-length) homodimer (SAXS)[c]	180	56.2 ± 0.5

[a] R_g values were calculated using GNOM.
[b] Scattering parameters for full-length type IIβ holoenzyme are from Vigil *et al.* (27).
[c] Scattering parameters for free full-length RIIβ homodimer are from Vigil *et al.* (41).

The individual scattering profiles of each component of the type IIβ(1–280) holoenzyme complex were extracted using the COMPOST module of MULCh and then used to estimate the individual scattering parameters (Table 1) and the *P*(*r*) curves for each component of the complex (Figs. 2 and 3). Comparison of the extracted scattering profiles for RIIβ(1–280) homodimer in the holoenzyme complex with scattering for free homodimer determined using SAXS indicates that the RIIβ(1–280) homodimer in the holoenzyme is much more compact than the free homodimer (Table 1, Fig. 2*B*). The R_g of the free RIIβ(1–280) homodimer is 43.4 Å, which is significantly more extended than the R_g of 35.6 Å when the homodimer is bound to the C subunit in the type IIβ(1–280) holoenzyme complex (Table 1). There is a corresponding change in D_{max} of the RIIβ(1–280) homodimer from 140 to 110 Å upon forming the holoenzyme complex. These dramatic changes in R_g and D_{max} are much greater than the changes seen in the RIα homodimer when it binds C subunits (25).

The extracted C subunit scattering profiles were used to generate *P*(*r*) curves, which were compared with *P*(*r*) curves of C subunits in the previously studied RIα holoenzyme complex (25) (Fig. 2*C*). The *P*(*r*) curves indicate that the C subunits are much closer together in the type IIβ(1–280) holoenzyme than they are in the type Iα holoenzyme. The C subunits are also much closer to each other in the type IIβ(1–280) holoenzyme than in the type IIα holoenzyme complex (Ref. 29 and data not presented here). The D_{max} value for the C subunits in the RIα holoenzyme complex is 140 Å as compared with 115 Å for the D_{max} of the C subunits in the type IIβ(1–280) holoenzyme complex (Fig. 2*C*). The second peak in each of the two *P*(*r*) curves shown in Fig. 2*C* corresponds to the approximate distance between the centers of mass of C subunits in the two different holoenzymes (115 Å in type Iα and 70 Å in type IIβ(1–280)).

SAXS Analysis of the RIIβ(1–280) Homodimer as Compared with Full-length RIIβ Homodimer—Previous SAXS studies have shown that the solution structure of the full-length RIIβ homodimer structure is extended, similar to what is seen with the RIIα homodimer structure (41). SAXS analysis of the RIIβ(1–280) homodimer indicates that it is also relatively extended although it is significantly shorter than the full-length RIIβ homodimer (D_{max} = 140 Å *versus* 180 Å; Fig. 3*C*). Moreover, cAMP has relatively little effect on the solution structure of the RIIβ(1–280) homodimer (Fig. 3*C*). Similarly modest effects of cAMP on the solution structures of the RIα and RIIα homodimers were reported by Vigil *et al.* (41).

Modeling of Type IIβ(1–280) Holoenzyme Subunit Organization Based on SANS with Solvent Contrast Variation—Models of the type IIβ(1–280) holoenzyme were generated as described under "Experimental Procedures" using the SANS with solvent contrast variation data shown in Fig. 2*A* as target functions. The *solid line* on each scattering curve in Fig. 2*A* is the fit of the best-fit model shown in Fig. 4*A* (χ^2 = 0.815), whereas the *dashed lines* show the range of the scattering profiles of the entire set of 75 models retained. As a starting point for the modeling, the R:C heterodimers from the crystal structure of the type IIβ holoenzyme (PDB: 3TNP) were used. The C-terminal CNB domains of the RIIβ subunits were removed from the 3TNP structure by editing the PDB file. Because the 3TNP structure is missing residues 1–103 of the RIIβ subunits, the structure corresponding to the D/D domain was added based on the D/D domain structure of RIIα (PDB: 2HWN), and the linker regions were modeled as a single cylindrical volume. As compared with one another (Fig. 4, *A-C*, and Fig. 5), the rigid body models produced from fitting the SANS data show some differences in the positions of the C and the R subunits relative

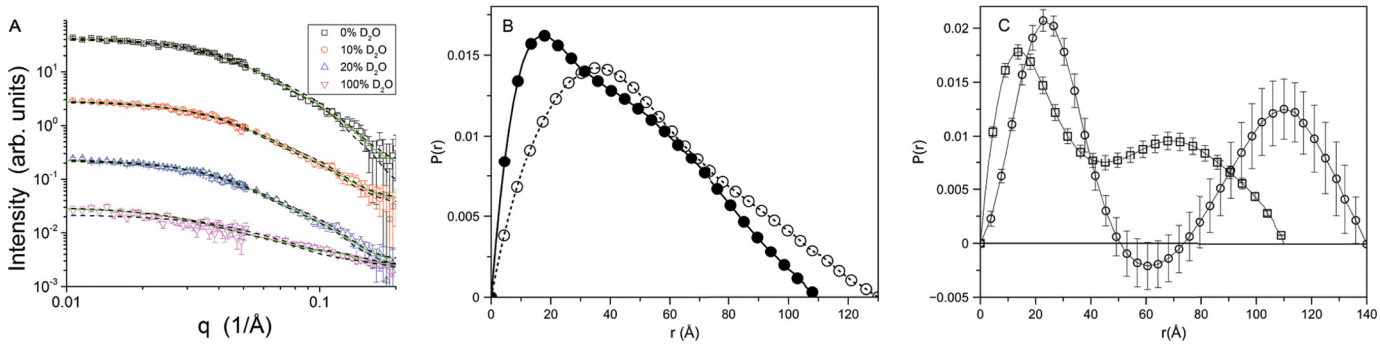

FIGURE 2. **Small angle neutron scattering of type IIβ(1–280) holoenzyme.** *A*, *I*(*q*) *versus q* plots of a neutron scattering solvent contrast series using type IIβ(1–280) holoenzyme containing deuterated C subunit. The *solid green lines* tracing through the scattering data points at each solvent contrast point are predicted scattering curves obtained from the type IIβ(1–280) holoenzyme structural model shown in Fig. 4*A*. The *dashed black lines* represent the range of predicted scattering curves of the 75 best-fit structural models. *arb. units*, arbitrary units. The scattering data were binned, and the *error bars* reflect neutron counting statistics and the S.D. of the data within the bin. *B*, *P*(*r*) function of RIIβ(1–280) homodimer in the holoenzyme complex (*filled circles*) was extracted from the SANS solvent contrast series using MULCh. The *P*(*r*) of free RIIβ(1–280) homodimer determined by SAXS (*open circles*) is shown for comparison. The size of the symbols is comparable to or larger than the estimated errors. *C*, *P*(*r*) functions of C subunits in the type IIβ(1–280) holoenzyme complex (*open squares*). The *P*(*r*) curve of the C subunits in the type Iα holoenzyme (*open circles* (25)) is shown for comparison.

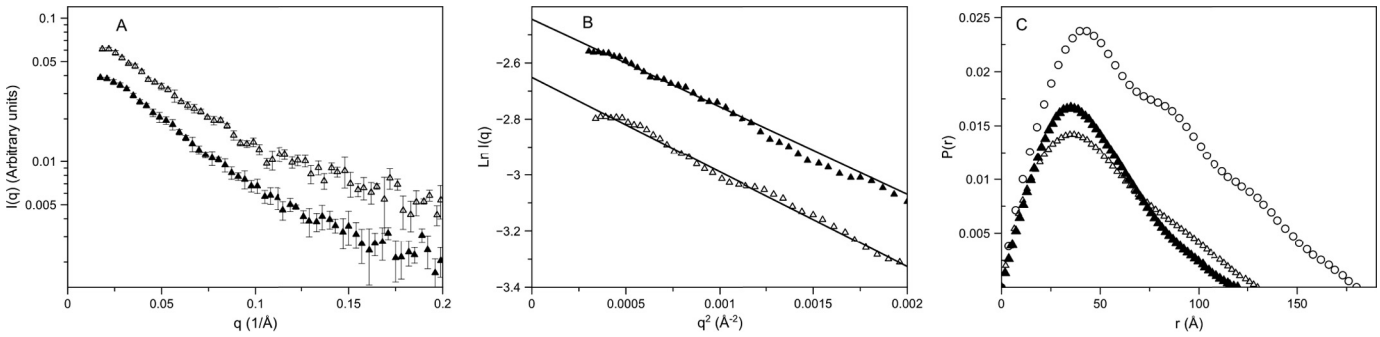

FIGURE 3. **Small angle x-ray scattering of RIIβ(1–280) homodimer.** *A*, *I*(*q*) *versus q* plots of free RIIβ(1–280) homodimer in the absence (*open triangles*) and presence (*filled triangles*) of cAMP. The scattering data were binned, and the *error bars* reflect the S.D. of the points within the bin. The *I*(*q*) scale is arbitrary, and the plots have been offset to facilitate comparison. *B*, Guinier plots of free RIIβ(1–280) homodimer in the absence (*open triangles*) and presence (*filled triangles*) of cAMP. The *I*(*q*) scale is arbitrary and has been offset to facilitate comparison. The line shown with each dataset is a linear fit to the data in the range from q_{min} to $q^2 = 0.0013$. This value of q^2 corresponds to $q \times R_g = 1.3$. *C*, *P*(*r*) functions for free RIIβ(1–280) homodimer in the absence (*open triangles*) and presence (*filled triangles*) of cAMP. The *P*(*r*) function of full-length RIIβ homodimer (from Ref. 41) is shown for comparison. The area under each curve has been scaled to reflect the square of molecular weight of the particle. Estimated errors are equal to or smaller than the symbols.

to one another, but overall, the C subunits are close together near the center of the complex with the N-terminal CNBD-A domains located slightly more to the periphery. As compared with the crystal structure (Fig. 4*D*) of tetrameric full-length type IIβ holoenzyme (PDB: 3TNP), the CNBD-A domains are located closer to the center of the complex in the crystal structure, and the overall structure appears to be more compact although the D/D domain and linker regions are not resolved in this structure.

DISCUSSION

The four PKA isoforms show very different patterns of homodimer and tetrameric holoenzyme solution structural properties as assessed by SAXS and SANS (27, 41). The RIIβ isoform is unique among the PKA isoforms in that its homodimer solution structure is extended and is similar in shape to the RIIα homodimer, but its holoenzyme solution structure is very compact and similar in shape to the RIα holoenzyme. An interesting question that can be answered by SANS with solvent contrast variation is whether the organization of subunits is similar in the compact solution structures of the type IIβ and type Iα holoenzymes. In addition, the RIIβ-(1–280) construct allows us to answer questions regarding the relative contributions of the D/D domain, the linker, and the CNBDs to the unique pattern of the homodimer and holoenzyme structures of the RIIβ isoform. The compact dimensions of the type IIβ(1–280) holoenzyme solution structure determined in the present study indicate that the compact structure of the type IIβ holoenzyme does not require the C-terminal CNBD-B domain. The truncated RIIβ(1–280) homodimer shows a similar compaction upon forming a holoenzyme complex as the full-length RIIβ homodimer, going from a D_{max} of 140 to 110 Å, and a decrease in R_g from 43.4 to 35.6 Å (Table 1). Thus, the minimal structural elements needed to form a tetrameric holoenzyme complex (the D/D domain, linker, and CNBD-A) are sufficient to form a compact type IIβ holoenzyme structure.

The compact holoenzyme solution structure seen with SAXS and SANS is consistent with the compact structure of the recently described full-length RIIβ tetrameric holoenzyme crystal structure (22). The type IIβ holoenzyme crystal structure implicates the CNBD-A domain as being critical in forming a compact structure through interactions of the β4-β5 loop of each CNBD-A domain with the C subunit in the opposing heterodimer. In contrast, the CNBD-B domains are positioned

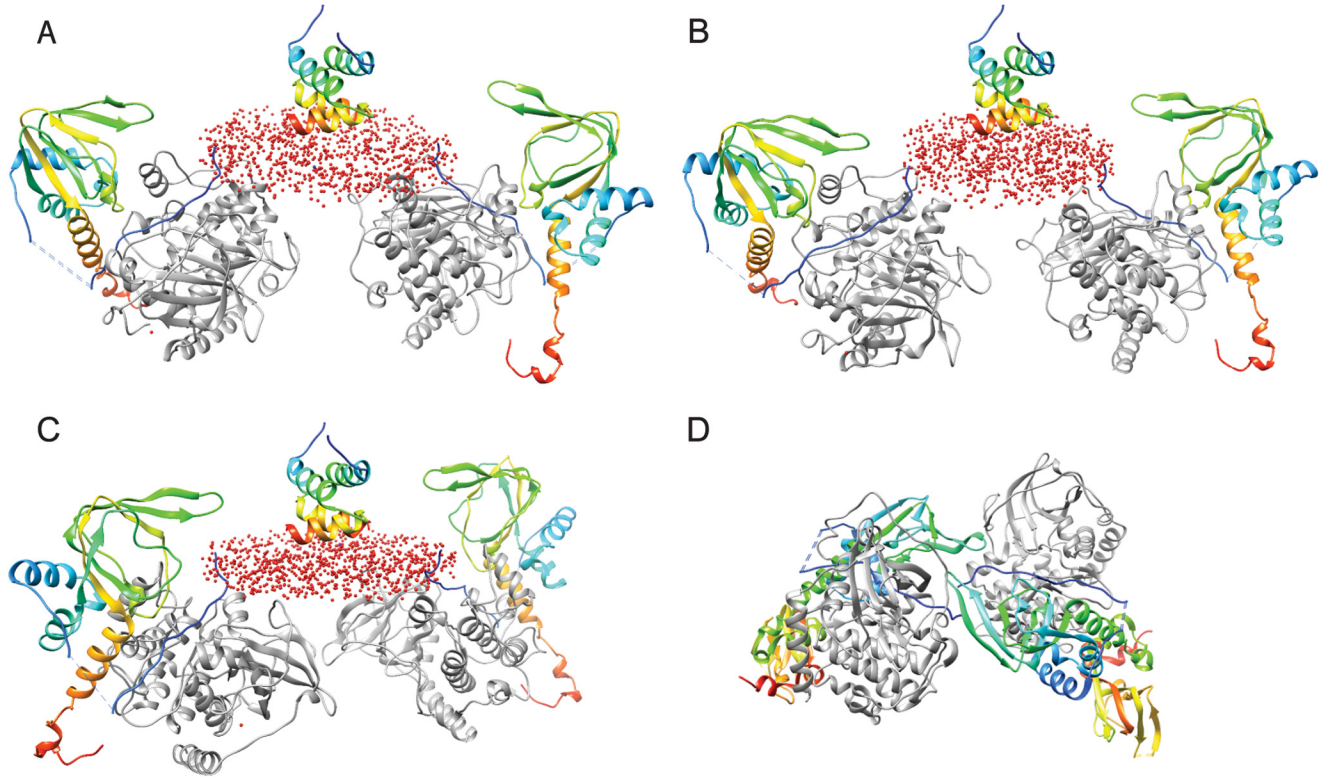

FIGURE 4. **Best-fit models of type IIβ(1–280) holoenzyme based on neutron scattering with solvent contrast.** Models were generated as described under "Experimental Procedures" using data from the SANS solvent contrast series shown in Fig. 2. The models were generated using the D/D domain structure of RIIα (PDB: 2HWN) and the RIIβ(104–280)-C(14–350) heterodimers from the structure of type IIβ holoenzyme (PDB: 3TNP). The linker regions are modeled as a single cylinder to simulate the volume occupied by this region of the protein. The chains in the R subunit domains are colored with N termini in *blue* and C termini in *red*. The C subunits are colored *gray*, and the volume corresponding to the linkers is depicted as a *red cylindrical cloud*. *A–C*, the model with the best χ-square fit to the SANS data is shown ($\chi^2 = 0.815$) *panel A* with two other independently determined models shown in *panels B* ($\chi^2 = 0.817$) and *C* ($\chi^2 = 0.821$). The predicted neutron scattering curves from the model in *panel A* are shown as the *solid green lines* in Fig. 2 as compared with the experimental neutron scattering. *D*, the structure is the crystal structure of the type IIβ tetramer formed with full-length RIIβ (PDB: 3TNP); it is arbitrarily oriented relative to the models. Molecular graphics for this figure were prepared with the UCSF Chimera package. Chimera is developed by the Resource for Biocomputing, Visualization, and Informatics at the University of California, San Francisco (supported by National Institutes of Health Grant P41-GM103311 through the NIGMS) (42).

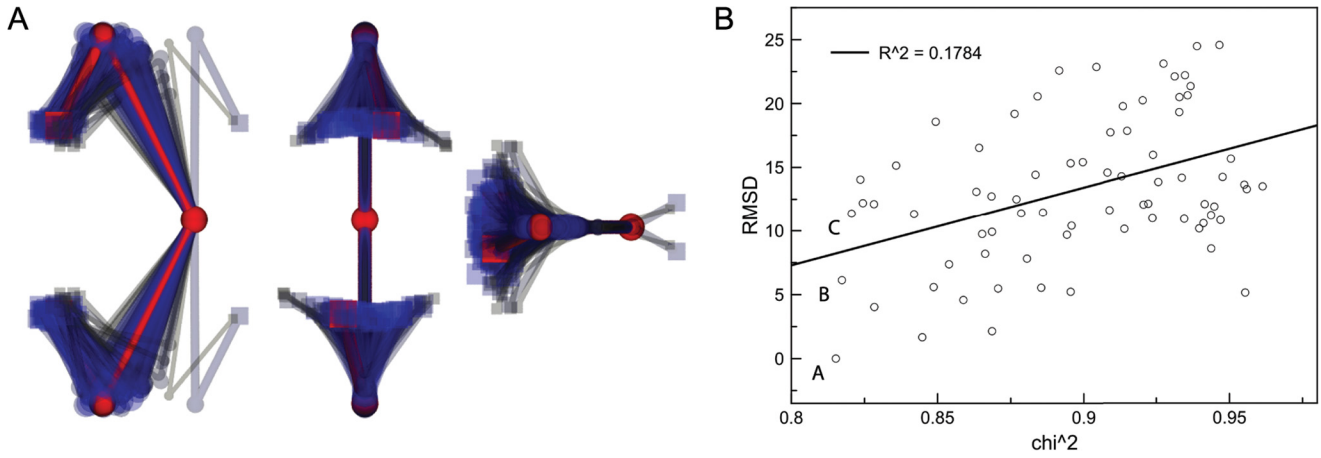

FIGURE 5. **Comparison of the 75 best-fit models.** *A*, the 75 best-fit models were compared by overlaying all of the models based on the centers of mass of the C subunits (*boxes*), the CNBD-A of the R subunits (*spheres toward the periphery*), and the D/D domain of the R subunits (*spheres near the center*). The models were aligned by rotating them around the *z* axis such that the *y*-coordinates of the centers of mass of the R subunits are all 0.00. Three orthogonal views of the overlaid models are shown. The lowest χ^2 model (Fig. 4*A*) is shown in *red*, and the other models are shown in transparent shades ranging from *blue* to *gray* with the lowest χ^2 models being *blue* and the highest χ^2 models being *gray*. *B*, root mean squared deviation (*RMSD*) relative to the lowest χ-squared model as a function of χ^2 value. The points with the three lowest χ^2 values are labeled as *A*, *B*, and *C* and correspond to the models shown in Fig. 4, *A–C*, respectively. The *solid line* is a linear regression fit to the data and shows that there is only a weak correlation ($r^2 = 0.1784$) between χ^2 and root mean squared deviation to the lowest χ^2 model. Root mean squared deviation values were calculated by the program DAMCLUST (43) using the all atom, P2 symmetry, and handedness options.

toward the periphery of the complex and do not interact with the opposing heterodimer (Fig. 4*D*). Interestingly, the predicted *P*(*r*) curve of the C subunits in the full-length type IIβ holoenzyme crystal structure indicates that the C subunits are closer together in the crystal structure than they are in the solution structure of the type IIβ(1–280) holoenzyme. This greater sep-

aration of C subunits in the solution structure of the type IIβ(1–280) holoenzyme is also seen in the best-fitting models presented in Fig. 4. It is not clear whether the less compact C subunit organization observed by SANS in the type IIβ(1–280) holoenzyme is due to the lack of the CNBD-B domains or the result of increased mobility of the R:C heterodimers when the holoenzyme is in solution. In addition to the CNBD-A domains, it is likely that the RIIβ linker also plays an essential role in organizing the compact type IIβ tetrameric structure based on previous SAXS studies by Vigil *et al.* (27). Those studies showed that a tetrameric holoenzyme formed with an RIIα/RIIβ chimeric mutant in which part of the RIIβ linker and the D/D domain were replaced with those elements from RIIα, had a much more extended structure than the wild-type type IIβ holoenzyme complex, but somewhat more compact structure than wild-type type IIα holoenzyme (27).

Because the type Iα holoenzyme complex has also been studied by SANS (25), the present study affords an opportunity to compare the organization of C subunits within two different PKA isoforms that both form compact R_2:C_2 holoenzyme complexes. As shown in Fig. 2*C*, the *P*(*r*) curves of the C subunit extracted from the SANS solvent contrast series are dramatically different for the type Iα holoenzyme and the type IIβ(1–280) holoenzyme. The second peak in the *P*(*r*) curve of the C subunits is dominated by vector lengths between the two C subunits in the complex and indicates that the C subunits are ~40 Å farther apart in the type Iα holoenzyme than in the type IIβ(1–280) holoenzyme. This altogether different structural organization of C subunits in these two compact PKA holoenzymes must give rise to very different kinds of structural rearrangements during the activation and inactivation of these two PKA isoforms. In the case of RIα, the free homodimer is a compact structure that is likely to form a relatively stable scaffold for C subunit binding. Enzyme activation and inactivation would entail minimal structural rearrangement of the RIα homodimer. Indeed, the *P*(*r*) profile of free RIα homodimer determined by SAXS is rather similar to the *P*(*r*) profile of the RIα homodimer bound to C subunits determined by SANS (25), supporting the idea that the RIα homodimer undergoes minimal conformational rearrangement when it binds or dissociates from the C subunits. In contrast, the free RIIβ and RIIβ(1–280) homodimer structures are very extended (Fig. 3*C*) and thus must undergo a large structural rearrangement, presumably involving the D/D domain, linker, and CNBD-A, to form the much more compact structure that is indicated by the basic scattering parameters (Table 1) and *P*(*r*) curves derived from SANS measurements of the type IIβ(1–280) holoenzyme (Fig. 2*B*). This more complex structural rearrangement of the RIIβ homodimer occurring during activation and inactivation of the type IIβ isoform is likely to play a biologically important role in type IIβ function such as facilitating communication from the D/D domain to the linker, CNBD-A, and C subunits. Such intramolecular communication within the type IIβ holoenzyme could give rise to very different activation and inactivation dynamics depending upon the AKAP to which the enzyme is bound. Regulation of RIIβ autophosphorylation (which lowers R affinity for C) via AKAP-bound protein phosphatases could provide an additional layer of regulatory control of type IIβ activation and inactivation in different AKAP-mediated signaling complexes. Small angle neutron and x-ray scattering studies are currently in progress to assess the role of AKAP interactions on RIIβ structure in such AKAP-mediated multienzyme signaling complexes.

Acknowledgments—We thank Dr. Jill Trewhella for the generous use of small angle x-ray scattering and laboratory facilities at the University of Utah. X-ray scattering data were collected at the University of Utah using facilities that were supported by U.S. Department of Energy Grant DE-FG02-05ER64026 (to Jill Trewhella). The Center for Structural Molecular Biology operates BioSANS and is supported by the U.S. Department of Energy, Office of Science, Office of Biological and Environmental Research Project ERKP291. The High Flux Isotope Reactor is sponsored by the Scientific User Facilities Division, Basic Energy Sciences. Oak Ridge National Laboratory (ORNL) is managed by UT-Battelle, LLC, for the U.S. Department of Energy (DOE) under Contract DE-AC05-00OR22725.

REFERENCES

1. Soderling, T. R., Hickenbottom, J. P., Reimann, E. M., Hunkeler, F. L., Walsh, D. A., and Krebs, E. G. (1970) Inactivation of glycogen synthetase and activation of phosphorylase kinase by muscle adenosine 3′,5′-monophosphate-dependent protein kinases. *J. Biol. Chem.* **245,** 6317–6328
2. McDonald, T. F., Pelzer, S., Trautwein, W., and Pelzer, D. J. (1994) Regulation and modulation of calcium channels in cardiac, skeletal, and smooth muscle cells. *Physiol. Rev.* **74,** 365–507
3. Wang, J. Q., Liu, X., Zhang, G., Parelkar, N. K., Arora, A., Haines, M., Fibuch, E. E., and Mao, L. (2006) Phosphorylation of glutamate receptors: a potential mechanism for the regulation of receptor function and psychostimulant action. *J. Neurosci. Res.* **84,** 1621–1629
4. Shaywitz, A. J., and Greenberg, M. E. (1999) CREB: a stimulus-induced transcription factor activated by a diverse array of extracellular signals. *Annu. Rev. Biochem.* **68,** 821–861
5. Kirschner, L. S., Carney, J. A., Pack, S. D., Taymans, S. E., Giatzakis, C., Cho, Y. S., Cho-Chung, Y. S., and Stratakis, C. A. (2000) Mutations of the gene encoding the protein kinase A type I-α regulatory subunit in patients with the Carney complex. *Nat. Genet.* **26,** 89–92
6. Groussin, L., Jullian, E., Perlemoine, K., Louvel, A., Leheup, B., Luton, J. P., Bertagna, X., and Bertherat, J. (2002) Mutations of the *PRKAR1A* gene in Cushing's syndrome due to sporadic primary pigmented nodular adrenocortical disease. *J. Clin. Endocrinol. Metab.* **87,** 4324–4329
7. Beuschlein, F., Fassnacht, M., Assié, G., Calebiro, D., Stratakis, C. A., Osswald, A., Ronchi, C. L., Wieland, T., Sbiera, S., Faucz, F. R., Schaak, K., Schmittfull, A., Schwarzmayr, T., Barreau, O., Vezzosi, D., Rizk-Rabin, M., Zabel, U., Szarek, E., Salpea, P., Forlino, A., Vetro, A., Zuffardi, O., Kisker, C., Diener, S., Meitinger, T., Lohse, M. J., Reincke, M., Bertherat, J., Strom, T. M., and Allolio, B. (2014) Constitutive activation of PKA catalytic subunit in adrenal Cushing's syndrome. *N. Engl. J. Med.* **370,** 1019–1028
8. Cao, Y., He, M., Gao, Z., Peng, Y., Li, Y., Li, L., Zhou, W., Li, X., Zhong, X., Lei, Y., Su, T., Wang, H., Jiang, Y., Yang, L., Wei, W., Yang, X., Jiang, X., Liu, L., He, J., Ye, J., Wei, Q., Li, Y., Wang, W., Wang, J., and Ning, G. (2014) Activating hotspot L205R mutation in *PRKACA* and adrenal Cushing's syndrome. *Science* **344,** 913–917
9. Goh, G., Scholl, U. I., Healy, J. M., Choi, M., Prasad, M. L., Nelson-Williams, C., Kunstman, J. W., Korah, R., Suttorp, A. C., Dietrich, D., Haase, M., Willenberg, H. S., Stålberg, P., Hellman, P., Akerström, G., Björklund, P., Carling, T., and Lifton, R. P. (2014) Recurrent activating mutation in *PRKACA* in cortisol-producing adrenal tumors. *Nat. Genet.* **46,** 613–617
10. Sato, Y., Maekawa, S., Ishii, R., Sanada, M., Morikawa, T., Shiraishi, Y., Yoshida, K., Nagata, Y., Sato-Otsubo, A., Yoshizato, T., Suzuki, H., Shiozawa, Y., Kataoka, K., Kon, A., Aoki, K., Chiba, K., Tanaka, H., Kume, H., Miyano, S., Fukayama, M., Nureki, O., Homma, Y., and Ogawa, S. (2014) Recurrent somatic mutations underlie corticotropin-independent Cush-

ing's syndrome. *Science* **344,** 917–920
11. Cho, Y. S., Park, Y. G., Lee, Y. N., Kim, M. K., Bates, S., Tan, L., and Cho-Chung, Y. S. (2000) Extracellular protein kinase A as a cancer biomarker: its expression by tumor cells and reversal by a myristate-lacking Cα and RIIβ subunit overexpression. *Proc. Natl. Acad. Sci. U.S.A.* **97,** 835–840
12. Gordge, P. C., Hulme, M. J., Clegg, R. A., and Miller, W. R. (1996) Elevation of protein kinase A and protein kinase C activities in malignant as compared with normal human breast tissue. *Eur. J. Cancer* **32A,** 2120–2126
13. Naviglio, S., Di Gesto, D., Illiano, F., Chiosi, E., Giordano, A., Illiano, G., and Spina, A. (2010) Leptin potentiates antiproliferative action of cAMP elevation via protein kinase A down-regulation in breast cancer cells. *J. Cell Physiol.* **225,** 801–809
14. Beristain, A. G., Molyneux, S. D., Joshi, P. A., Pomroy, N. C., Di Grappa, M. A., Chang, M. C., Kirschner, L. S., Privé, G. G., Pujana, M. A., and Khokha, R. (2014) PKA signaling drives mammary tumorigenesis through Src. *Oncogene* 10.1038/onc.2014.41
15. Chen, L., Marquardt, M. L., Tester, D. J., Sampson, K. J., Ackerman, M. J., and Kass, R. S. (2007) Mutation of an A-kinase-anchoring protein causes long-QT syndrome. *Proc. Natl. Acad. Sci. U.S.A.* **104,** 20990–20995
16. Molkentin, J. D., and Dorn, G. W., 2nd. (2001) Cytoplasmic signaling pathways that regulate cardiac hypertrophy. *Annu. Rev. Physiol.* **63,** 391–426
17. Vest, J. A., Wehrens, X. H., Reiken, S. R., Lehnart, S. E., Dobrev, D., Chandra, P., Danilo, P., Ravens, U., Rosen, M. R., and Marks, A. R. (2005) Defective cardiac ryanodine receptor regulation during atrial fibrillation. *Circulation* **111,** 2025–2032
18. Jicha, G. A., Weaver, C., Lane, E., Vianna, C., Kress, Y., Rockwood, J., and Davies, P. (1999) cAMP-dependent protein kinase phosphorylations on tau in Alzheimer's disease. *J. Neurosci.* **19,** 7486–7494
19. Lin, J. T., Chang, W. C., Chen, H. M., Lai, H. L., Chen, C. Y., Tao, M. H., and Chern, Y. (2013) Regulation of feedback between protein kinase A and the proteasome system worsens Huntington's disease. *Mol. Cell Biol.* **33,** 1073–1084
20. Marambaud, P., Chevallier, N., Ancolio, K., and Checler, F. (1998) Post-transcriptional contribution of a cAMP-dependent pathway to the formation of α- and β/γ-secretases-derived products of βAPP maturation in human cells expressing wild-type and Swedish mutated βAPP. *Mol. Med.* **4,** 715–723
21. Akimoto, M., Selvaratnam, R., McNicholl, E. T., Verma, G., Taylor, S. S., and Melacini, G. (2013) Signaling through dynamic linkers as revealed by PKA. *Proc. Natl. Acad. Sci. U.S.A.* **110,** 14231–14236
22. Zhang, P., Smith-Nguyen, E. V., Keshwani, M. M., Deal, M. S., Kornev, A. P., and Taylor, S. S. (2012) Structure and allostery of the PKA RIIβ tetrameric holoenzyme. *Science* **335,** 712–716
23. Taylor, S. S., Ilouz, R., Zhang, P., and Kornev, A. P. (2012) Assembly of allosteric macromolecular switches: lessons from PKA. *Nat. Rev. Mol. Cell Biol.* **13,** 646–658
24. Scott, J. D., Dessauer, C. W., and Taskén, K. (2013) Creating order from chaos: cellular regulation by kinase anchoring. *Annu. Rev. Pharmacol. Toxicol.* **53,** 187–210
25. Heller, W. T., Vigil, D., Brown, S., Blumenthal, D. K., Taylor, S. S., and Trewhella, J. (2004) C subunits binding to the protein kinase A RIα dimer induce a large conformational change. *J. Biol. Chem.* **279,** 19084–19090
26. Ilouz, R., Bubis, J., Wu, J., Yim, Y. Y., Deal, M. S., Kornev, A. P., Ma, Y., Blumenthal, D. K., and Taylor, S. S. (2012) Localization and quaternary structure of the PKA RIβ holoenzyme. *Proc. Natl. Acad. Sci. U.S.A.* **109,** 12443–12448
27. Vigil, D., Blumenthal, D. K., Taylor, S. S., and Trewhella, J. (2006) Solution scattering reveals large differences in the global structures of type II protein kinase A isoforms. *J. Mol. Biol.* **357,** 880–889
28. Zawadzki, K. M., and Taylor, S. S. (2004) cAMP-dependent protein kinase regulatory subunit type IIβ: active site mutations define an isoform-specific network for allosteric signaling by cAMP. *J. Biol. Chem.* **279,** 7029–7036
29. Zhao, J., Hoye, E., Boylan, S., Walsh, D. A., and Trewhella, J. (1998) Quaternary structures of a catalytic subunit-regulatory subunit dimeric complex and the holoenzyme of the cAMP-dependent protein kinase by neutron contrast variation. *J. Biol. Chem.* **273,** 30448–30459
30. Wall, M. E., Gallagher, S. C., and Trewhella, J. (2000) Large-scale shape changes in proteins and macromolecular complexes. *Annu. Rev. Phys. Chem.* **51,** 355–380
31. Vigil, D., Blumenthal, D. K., Brown, S., Taylor, S. S., and Trewhella, J. (2004) Differential effects of substrate on type I and type II PKA holoenzyme dissociation. *Biochemistry* **43,** 5629–5636
32. Herberg, F. W., Bell, S. M., and Taylor, S. S. (1993) Expression of the catalytic subunit of cAMP-dependent protein kinase in *Escherichia coli*: multiple isozymes reflect different phosphorylation states. *Protein Eng.* **6,** 771–777
33. Svergun, D. I. (1992) Determination of the regularization parameter in indirect-transform methods using perceptual criteria. *J. Appl. Crystallogr.* **25,** 495–503
34. Lynn, G. W., Heller, W., Urban, V., Wignall, G. D., Weiss, K., and Myles, D. A. A. (2006) Bio-SANS: a dedicated facility for neutron structural biology at Oak Ridge National Laboratory. *Physica B Condensed Matter* **385–386,** 880–882
35. Kline, S. R. (2006) Reduction and analysis of SANS and USANS data using IGOR Pro. *J. Appl. Crystallogr.* **39,** 895–900
36. Konarev, P. V., Volkov, V. V., Sokolova, A. V., Koch, M. H. J., and Svergun, D. I. (2003) PRIMUS: a Windows-PC based system for small-angle scattering data analysis. *J. Appl. Crystallogr.* **36,** 1277–1282
37. Whitten, A. E., Cai, S., and Trewhella, J. (2008) MULCh: ModULes for the analysis of small-angle neutron contrast variation data from biomolecular complexes. *J. Appl. Crystallogr.* **41,** 222–226
38. Tijoe, E., and Heller, W. T. (2007) ORNL_SAS: software for calculation of small-angle scattering intensities from bio-macromolecular structures. *J. Appl. Crystallogr.* **40,** 782–785
39. Heller, W. T. (2006) Ellstat: shape modelling for solution small-angle scattering of proteins and protein complexes with automated statistical characterization. *J. Appl. Crystallogr.* **39,** 671–675
40. Ibel, K., and Sturhmann, H. B. (1975) Comparison of neutron and X-ray scattering of dilute myoglobin solutions. *J. Mol. Biol.* **93,** 255–265
41. Vigil, D., Blumenthal, D. K., Heller, W. T., Brown, S., Canaves, J. M., Taylor, S. S., and Trewhella, J. (2004) Conformational differences among solution structures of the type Iα, IIα and IIβ protein kinase A regulatory subunit homodimers: role of the linker regions. *J. Mol. Biol.* **337,** 1183–1194
42. Pettersen, E. F., Goddard, T. D., Huang, C. C., Couch, G. S., Greenblatt, D. M., Meng, E. C., and Ferrin, T. E. (2004) UCSF Chimera: a visualization system for exploratory research and analysis. *J. Comput. Chem.* **25,** 1605–1612
43. Petoukhov, M. V., Franke, D., Shkumatov, A. V., Tria, G., Kikhney, A. G., Gajda, M., Gorba, C., Mertens, H. D. T., Konarev, P. V., and Svergun, D. I. (2012) New developments in the ATSAS program package for small-angle scattering data analysis. *J. Appl. Crystallogr.* **45,** 342–350